Supporting Information

# $MnCO_3$-Au Nanoparticles to Enable Catalytic Tumor Inhibition with Immune Activation

*Yingpei Yao ‡[a], Zijie Lu ‡[b], Yike Fu[a, c] *, Xiang Li[a, c] **

[a] State Key Laboratory of Silicon and Advanced Semiconductor Materials, School of Materials Science and Engineering, Zhejiang University, Hangzhou 310058, P. R. China

[b] Innovation Institute for Artificial Intelligence in Medicine, Zhejiang University, Hangzhou 310018, P. R. China

[c] ZJU-Hangzhou Global Science and Technology Innovation Center, Zhejiang University, Hangzhou 311215, P. R. China

* Corresponding authors

E-mail: fyk3927@zju.edu.cn (Y. Fu), xiang.li@zju.edu.cn (X. Li)

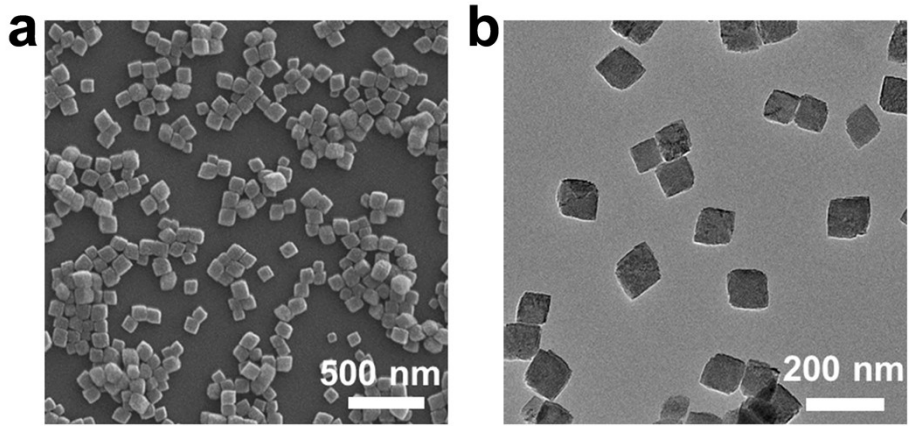


**Figure S1.** (a) SEM image and (b) TEM image of $MnCO_3$ nanoparticles.

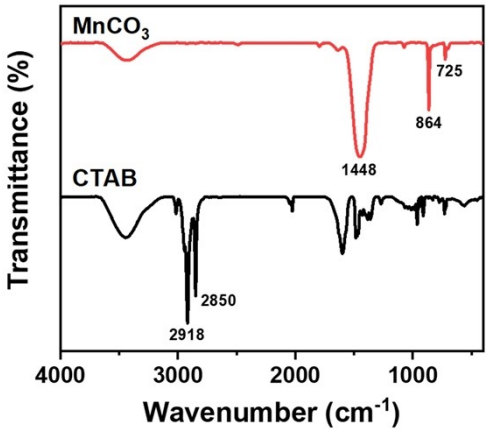


**Figure S2.** FTIR spectra of CTAB and as-prepared $MnCO_3$ nanoparticles.

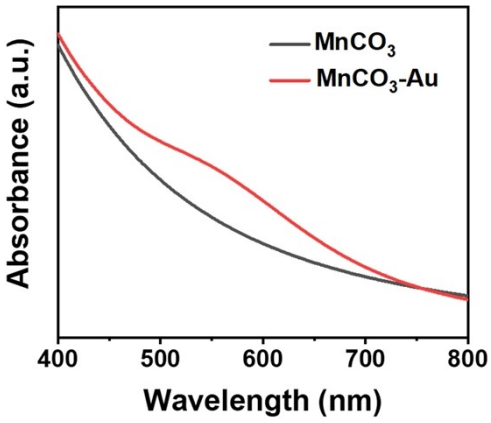


**Figure S3.** UV-Vis spectra of $MnCO_3$ and $MnCO_3$-Au.

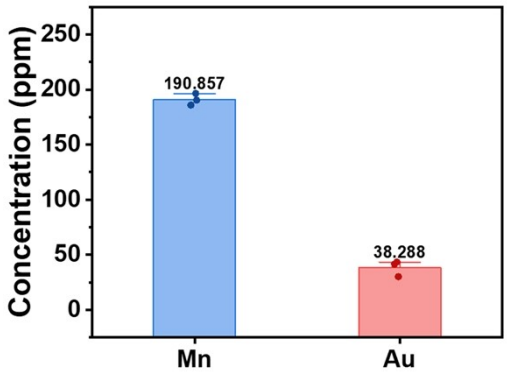


**Figure S4.** The concentrations of Mn and Au in the digestion solution of $MnCO_3$-Au nanoparticles determined by ICP-OES.

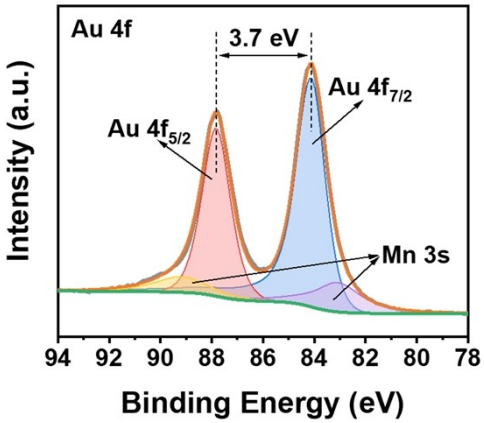


**Figure S5.** High-resolution Au 4f XPS spectrum of $MnCO_3$-Au.

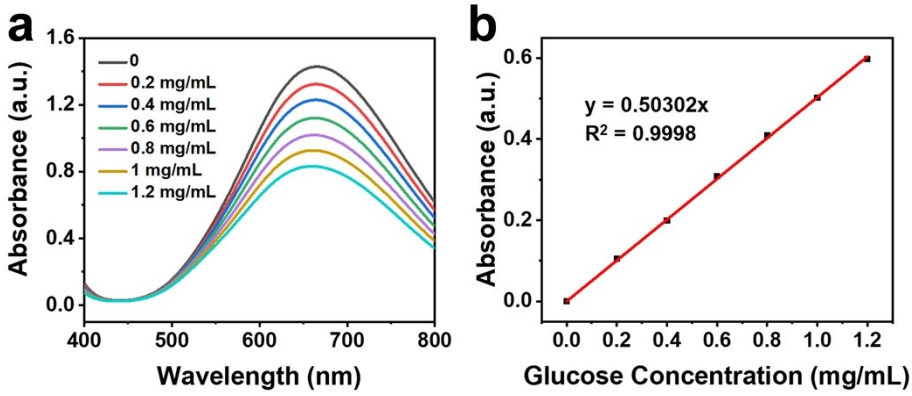


**Figure S6.** (a) UV-Vis absorption spectra of Fehling's reagent reacted with different concentrations of glucose. (b) The standard curve of absorbance difference at 663 nm versus glucose concentration.

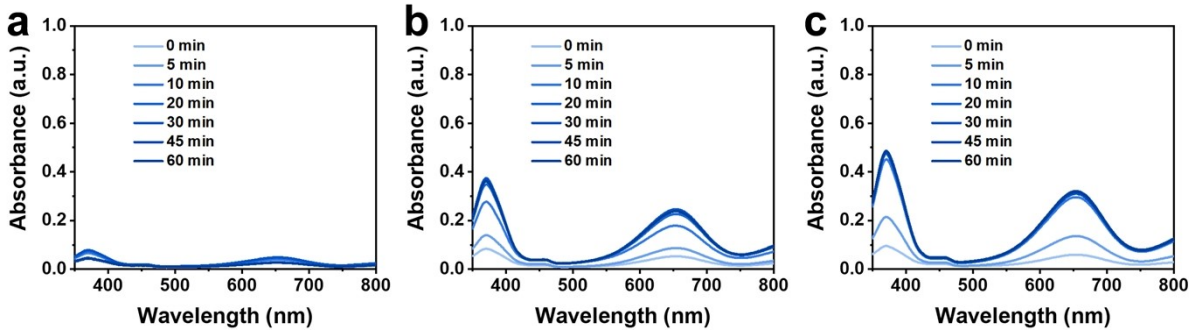


**Figure S7.** UV-Vis absorption spectra of TMB oxidized by generated $H_2O_2$ in (a) 0 mg/mL, (b) 0.5 mg/mL, and (c) 1 mg/mL glucose solutions at different time points with the addition of 500 μg/mL $MnCO_3$-Au.

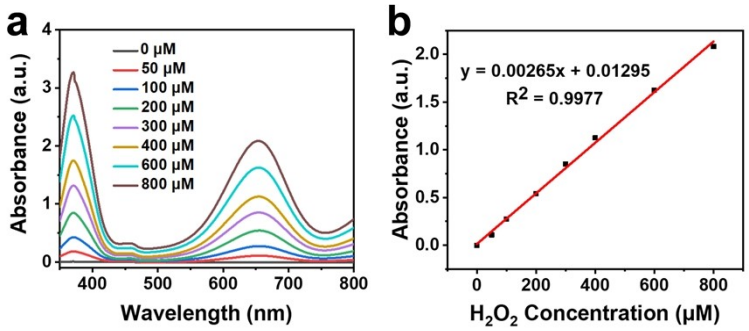


**Figure S8.** (a) UV-Vis absorption spectra of TMB oxidized by various concentrations of $H_2O_2$. (b) The standard curve of absorbance at 652 nm versus $H_2O_2$ concentration.

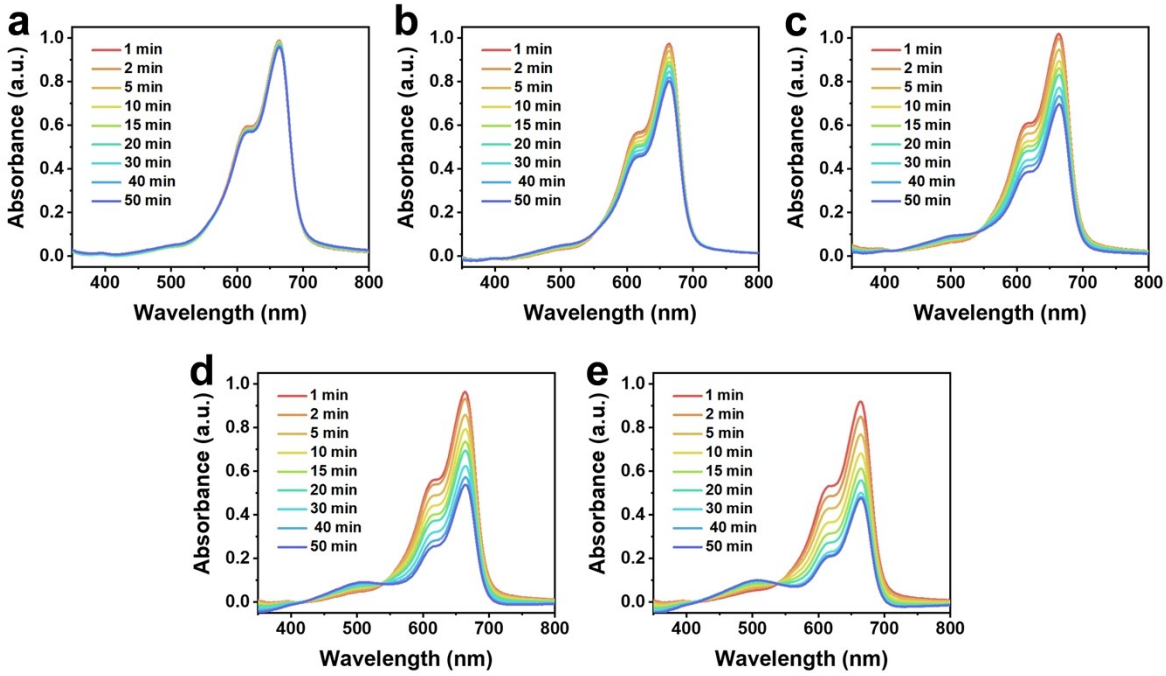


**Figure S9.** UV-Vis absorption spectra of MB solutions containing 500 μg/mL $MnCO_3$-Au and (a) 0 mg/mL, (b) 0.1 mg/mL, (c) 0.3 mg/mL, (d) 0.5 mg/mL, (e) 1 mg/mL glucose.

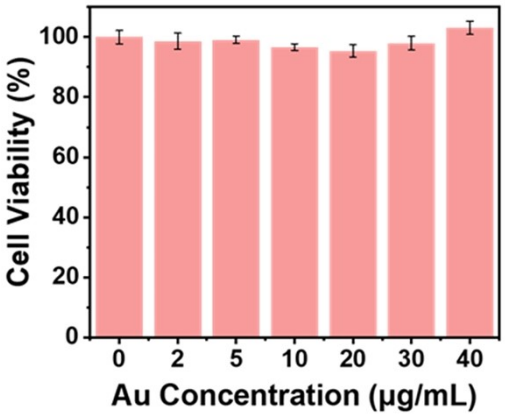


**Figure S10.** 4T1 cell viabilities after incubation with different concentrations of AuNPs for 24 h.

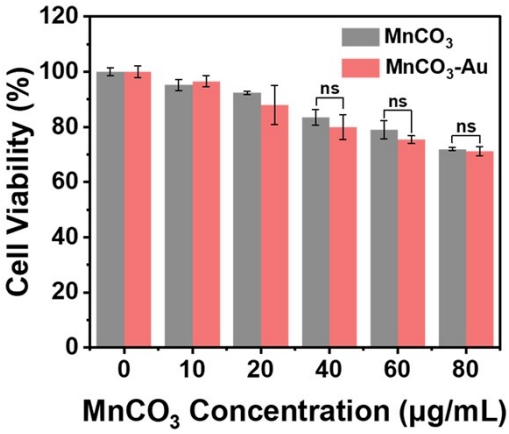


**Figure S11.** 4T1 cell viabilities after incubation with $MnCO_3$ and $MnCO_3$-Au in glucose-free RPMI 1640 medium.

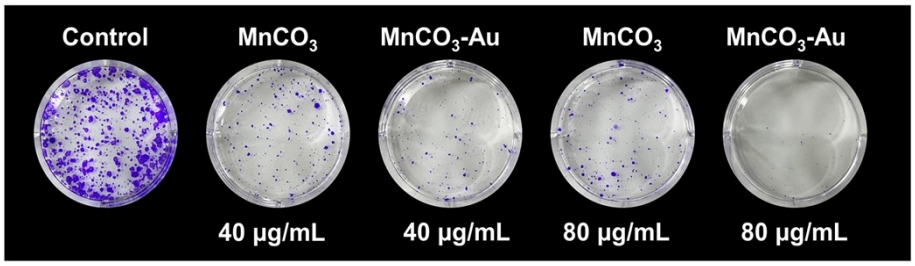


**Figure S12.** Colony formation of 4T1 cells after different treatments.

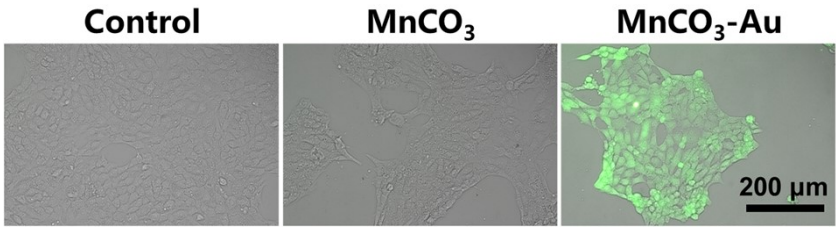


**Figure S13.** The bright-field images merged with fluorescence images of DCFH-DA stained 4T1 cells after being incubated with PBS, $MnCO_3$, and $MnCO_3$-Au.

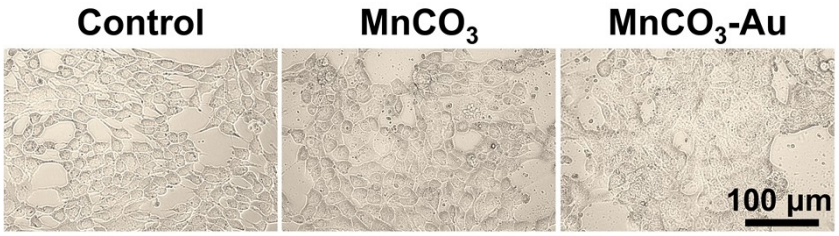


**Figure S14.** The bright-field images of JC-1 stained 4T1 cells after being treated with PBS, $MnCO_3$, and $MnCO_3$-Au.

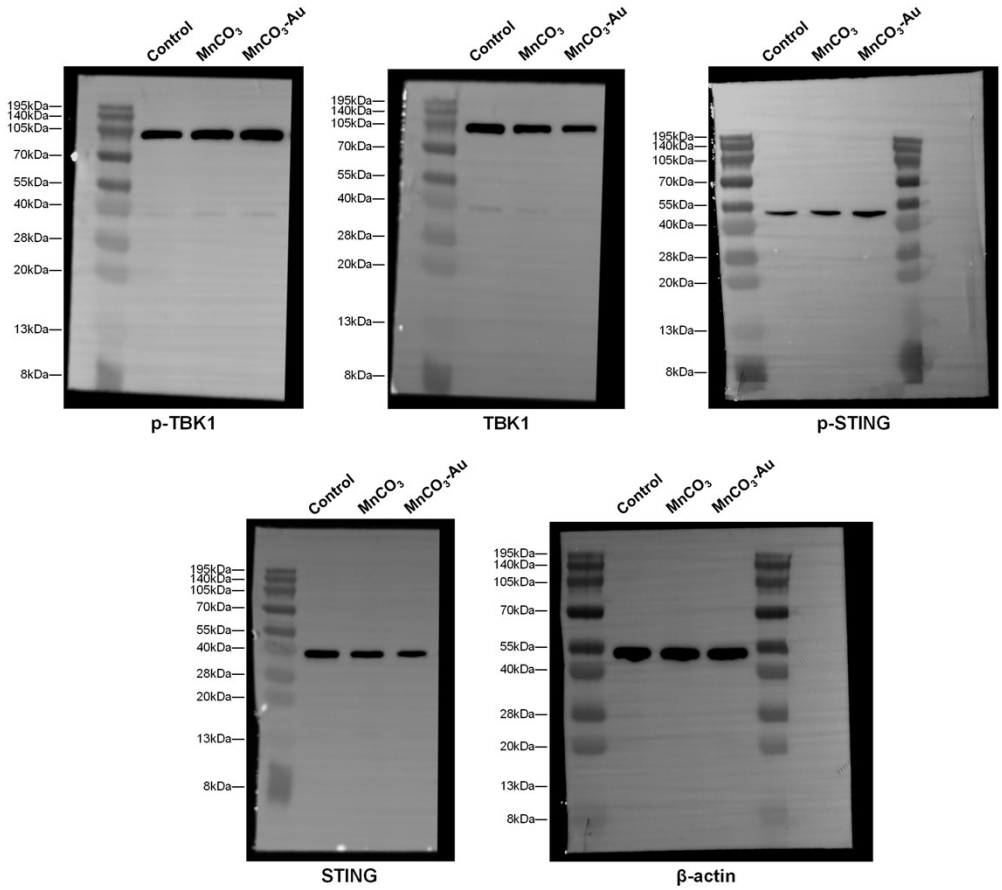


**Figure S15.** Raw data associated with Fig. 4d. Lanes were not cropped or rearranged when presenting the results in Fig. 4d.

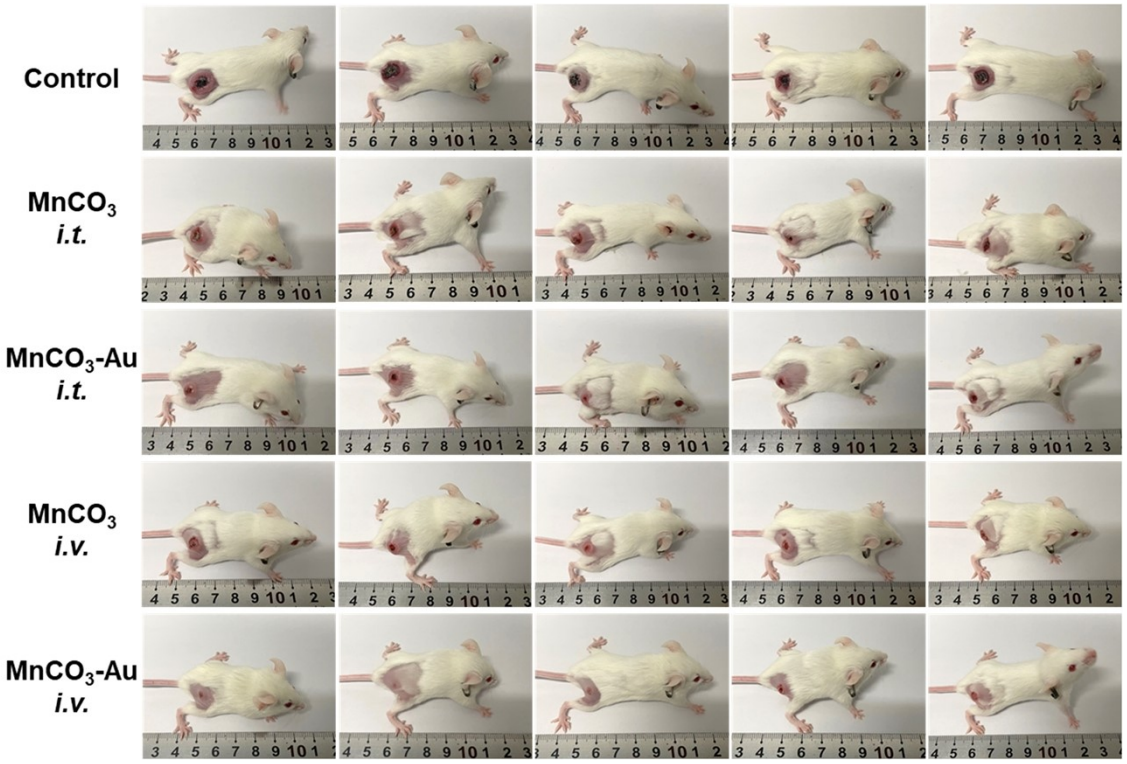


**Figure S16.** Photographs of tumor-bearing mice on day 14 after different treatments.

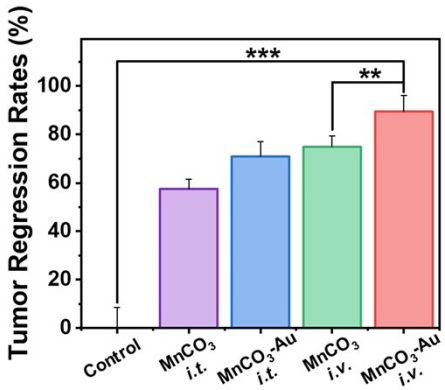


**Figure S17.** Tumor regression rates on day 14 after different treatments.

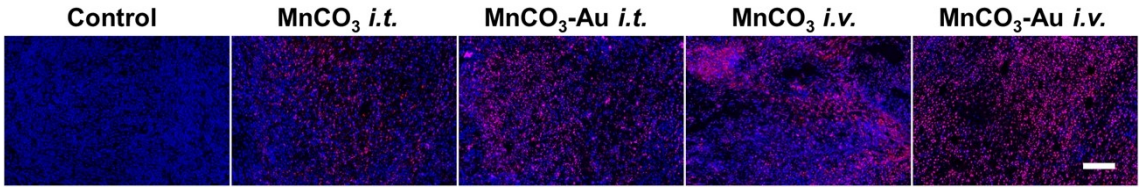


**Figure S18.** TUNEL immunofluorescence staining images of the tumors collected on day 14 after different treatments (scale bar: 100 μm).

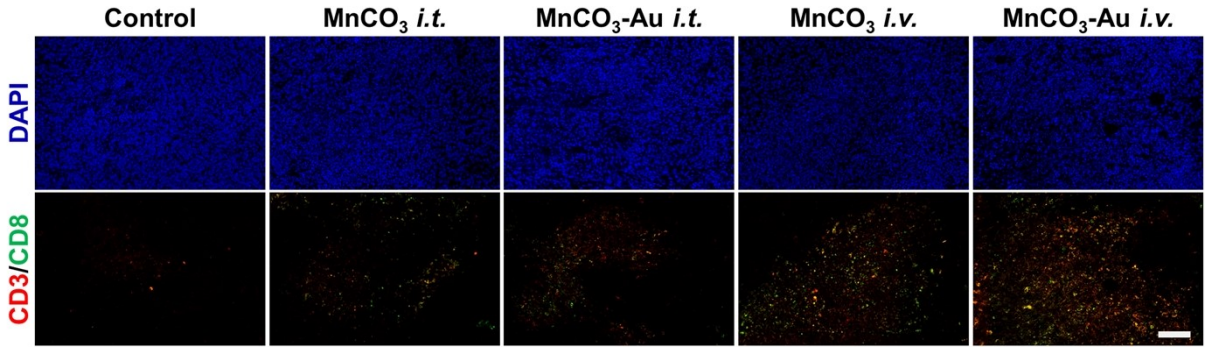


**Figure S19.** Immunofluorescence staining images of $CD8^+$ T cells in the tumors collected on day 14 after different treatments. CD3 is stained in red fluorescence and CD8 is stained in green fluorescence (scale bar: 100 μm).

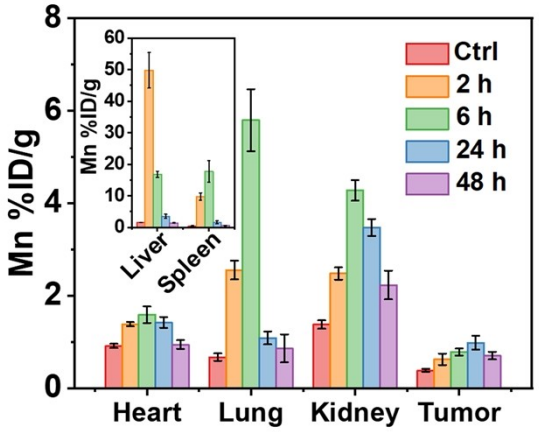


**Figure S20.** Biodistribution of Mn at various time points after intravenous injection of $MnCO_3$-Au ($n$ = 3, mean ± SD).

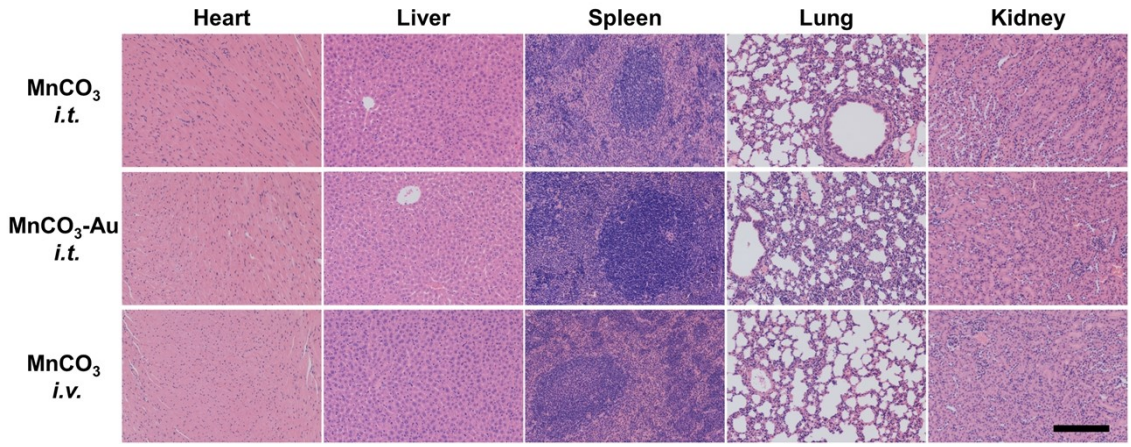


**Figure S21.** H&E staining images of major organs collected from mice after different treatments (scale bar: 200 μm).